COBEM 2023 27TH INTERNATIONAL CONGRESS OF MECHANICAL ENGINEERING

ABCM Brazilian Society of Mechanical Sciences and Engineering
27th ABCM International Congress of Mechanical Engineering
December 04-08, 2023, Florianópolis-SC, Brazil

COB-2023-2198
Intra-REV Pore Heterogeneity Model for Flow of Viscoplastic Material in Porous Media

Allan Barbosa Geoffroy Motta
Roney Leon Thompson
PEM/COPPE - Universidade Federal do Rio de Janeiro
abg.motta@mecanica.coppe.ufrj.br

Abstract. *Motivated by some discrepancies in the comparison between the pressure drop in plug scale experiments and continuum model simulations, we propose a model for the flow of viscoplastic material in porous media with a non-uniform pore distribution in the pore scale. The model employed is a continuum model that involves two scales. It is solved in the Darcy scale which requires information from the pore scale by a representative elementary volume (REV). The interaction between solid and fluid on the smallest scale is a key aspect and must be modeled via the interaction term. Usually, a pore geometry idealization is considered. The simplest geometry is the cylindrical pore, where an analytical solution for the interaction term can be obtained through some simplifications and the permeability is expected to be higher when compared to other geometries, so the pressure drop provided by this case would be the lowest possible. Despite that, in some cases, it is observed that the pressure drop predicted by the model is higher than the one observed in experiments. We aim to investigate this case considering a representative elementary volume composed of a non-uniform distribution of cylindrical pores and the flow of a viscoplastic material. We apply the Mixture Theory of Continuum Mechanics, which is able to provide a complete momentum balance for problems of flow in porous media, in contrast to Darcy's Law which is indicated only for low permeability regions. An analytical interaction term is developed for the Bingham viscoplastic material. Plug scale simulations are performed and we compare pressure drop between the representative REV idealized by a single pore and the REV idealized by a known non-uniform distribution of pores. From the results, it is clear that the pore heterogeneity is a possible source of discrepancy between the pressure drop from experiments and simulations.*

Keywords: *viscoplastic material, porous-media, mixture theory, CFD, pore size distribution*

1. INTRODUCTION

Numerous industrial applications involve the flow of non-Newtonian fluids through porous materials. One significant application is the acidizing process used to improve the permeability of a porous rock. In this scenario, the aim is to create channels, known as wormholes, that traverse the entire area while minimizing acid consumption (Wang *et al.*, 1993). Another common application in the oil industry is the elimination of residues from porous materials through fluid injection (Siddiqui *et al.*, 2006). Many of the fluids injected exhibit intricate rheological properties, such as shear rate dependency (Nasr-El-Din *et al.*, 2006). By utilizing polymer solutions, a viscoelastic behavior can be achieved (Alleman *et al.*, 2003). In certain applications, a fluid with complex behavior is desirable. Self-diverting fluid, a type of non-Newtonian acid, possesses the ability to treat non-preferential regions of porous media by locally adjusting its viscosity based on acid concentration. This adjustment can result in a temporary reduction in mobility (Chang *et al.*, 2001). The intricacy of the fluid has motivated the development of various models to address scenarios with and without acidification while considering the non-Newtonian nature of the fluids.

Various models are employed to deal with the challenge of flow in porous media, including network models, two-scale continuum models, and Lattice Boltzmann models. The two-scale continuum approach offers an alternative method that balances between accuracy of qualitative results and computational costs. Instead of solving the problem at the pore scale, this scale is modeled and the equations are solved at a higher scale known as the Darcy scale. As a result, the effectiveness of such a model heavily relies on assumptions made at the pore scale. Previous studies applied two-scale models to address the carbonate acidization problem (Liu *et al.*, 1997), (Golfier *et al.*, 2002). Liu *et al.* (1997) developed a model that produced qualitatively accurate predictions but was only applicable to the kinetic regime of the reaction. In contrast, Golfier *et al.* (2002) created a model suitable solely for cases with the mass-controlled regime. Panga *et al.* (2005) proposed a continuum model capable of accommodating both reaction regimes. Subsequently, Maheshwari *et al.* (2013) extended the application of the model to three-dimensional scenarios. Ratnakar *et al.* (2013) introduced non-Newtonian behavior into these models, motivated by the use of self-diverting fluids. One common simplification in these models pertains to the fluid momentum equation, often assuming pure Darcy's Law or expanding it with the inclusion of

the Brinkman term. Motta *et al.* (2021) later employed a comprehensive momentum equation based on Mixture Theory to investigate a plug acidification problem using a non-Newtonian fluid model.

The two-scale continuum approach employs a single representative pore to model flow at the pore scale, disregarding the significance of heterogeneity in porous media. For instance, Fletcher *et al.* (1991) conducted experiments to measure the apparent viscosity and observed that it was lower than the bulk viscosity in porous media. They attributed this phenomenon to slip effects and introduced a "rock factor," denoted as ξ, that depends on the porous matrix to compute the apparent shear rate. The measured plugs had ξ values ranging from 3.01 to 10.06. Furthermore, the expression for the apparent shear rate is derived from Blaze-Kozeny theory (Willhite and Uhl, 1988). However, Cannella *et al.* (1988) discovered that the apparent shear rate predicted by capillary bundle models did not align with the corresponding flow curve values. To address this discrepancy, they proposed an apparent shear rate function that incorporates a correction factor based on the fluid and porous media properties, enabling a match between the two quantities. Lopez *et al.* (2003) further discussed this matter, relating the apparent viscosity to the flow rate in a porous medium using a network model and considering a power-law fluid. Later, Motta *et al.* (2022) considered a two-scale continuum model with intra-REV heterogeneity to solve the problem of the flow of a power-law fluid. The apparent viscosity curves were closer to the bulk viscosity when the heterogeneity was considered.

In this study, we present a methodology for incorporating pore heterogeneity within the representative elementary volume (REV) of a two-scale model. This is achieved by considering a probability distribution of idealized pores with varying pore radii. The pore-scale assumptions are then incorporated into the Darcy-scale problem through the solid-fluid interaction term. To compare the results, simulations are conducted on a plug scale using the Bingham fluid model. Specifically, we examine the pressure drop results at a given flow rate. Furthermore, we investigate the influence of different distributions.

2. METHODOLOGY

2.1 Mixture-Theory

The fundamental basis of the Mixture Theory revolves around the notion that a mixture consists of multiple materials, with each material treated as a separate continuum (Atkin and Craine, 1976). The mixture can be seen as a combination of distinct continuum media, each possessing its own motion. At any given position and time, the mixture accommodates multiple constituents simultaneously. This conceptual framework enables the utilization of governing equations from Continuum Mechanics. Typically, the mixture's momentum balance is governed by a Cauchy equation. In the momentum equation for each constituent, a source term is incorporated to account for the internal forces between the constituents. The properties and constitutive relations employed in the momentum balance are attributed to individual constituents rather than the phase itself.

2.2 Darcy-Scale Model

In a porous medium, our two-scale continuum model is based on the Mixture Theory. The momentum balance for the fluid constituent is given by (Motta *et al.*, 2021)

$$\frac{\partial(\varepsilon\rho\mathbf{v})}{\partial t} + \nabla\cdot(\varepsilon\rho\mathbf{v}\mathbf{v}) = -\nabla(\varepsilon p) + \nabla\cdot(\varepsilon\boldsymbol{\tau}) + \mathbf{m}_f \tag{1}$$

where ε is the porosity, ρ is the mass density of the fluid, $\mathbf{v}$ is the intrinsic velocity vector, p is the pressure, $\boldsymbol{\tau}$ is the deviatoric part of the stress tensor, $\mathbf{m}_f$ is the interaction term. The interaction term represents the force per unit of volume that the fluid experiences due to the presence of the solid constituent. This term must be modeled with pore-scale assumptions and will be discussed later.

We considered a stress tensor given by the following form

$$\boldsymbol{\tau} = \tau_0 + \alpha\dot{\boldsymbol{\gamma}}, \tag{2}$$

where τ_0 is the yield stress, α is the viscosity when the stress in the fluid is above the yield stress, and $\dot{\boldsymbol{\gamma}}$ is the shear rate. The mass balance for the fluid constituent is given by:

$$\frac{\partial(\varepsilon\rho)}{\partial t} + \nabla\cdot(\varepsilon\rho\mathbf{v}) = 0, \tag{3}$$

2.3 Homogeneous pore-scale closures for Bingham material

The constitutive equation for a Bingham plastic in the scalar form is given by:

$$\tau = \tau_0 + \alpha\dot{\gamma} \tag{4}$$

Considering a REV made of an arrangement of passing cylinders with different radius. The interaction term is given by the volumetric density of the drag force in the pores.

$$\mathbf{m}_f = \frac{\mathbf{f}_t}{V_{REV}}. \tag{5}$$

The velocity profile in the permanent regime for a Bingham fluid in a pore, considering laminar, fully developed, and steady flow is given by:

$$v = \begin{cases} \frac{dp}{dx}\frac{R^2}{4\alpha}\left(1-\frac{R_p}{R}\right)^2, & 0 \le r \le R_p \\ \\ \frac{dp}{dx}\frac{R^2}{4\alpha}\left(1-\frac{r^2}{R^2}\right) - \frac{\tau_0}{\alpha}R\left(1-\frac{r}{R}\right), & R_p < r \le R \end{cases}$$

where R_p is the plug radius, τ_w is the wall shear stress. A force balance in the flow direction on a fluid element at a distance r can be written as:

$$\tau_{rz} = -\frac{\Delta p}{L}\frac{r}{2} \tag{6}$$

In the plug radius R_p, the equation (6) applies:

$$\tau_0 = -\frac{\Delta p}{L}\frac{R_p}{2} \tag{7}$$

The equation also applies to the wall shear stress:

$$\tau_w = -\frac{\Delta p}{L}\frac{R}{2} \tag{8}$$

The ratio τ_0/τ_w is then given by:

$$\frac{\tau_0}{\tau_w} = \frac{R_p}{R} \tag{9}$$

The flow rate Q is given by:

$$Q = \frac{\pi R^4}{8\alpha}\frac{dp}{dx}\left(1-\frac{4}{3}\phi+\frac{1}{3}\phi^4\right) \tag{10}$$

where $\phi = \tau_0/\tau_w$.
The average velocity is:

$$v_m = \frac{Q}{A} = \frac{R^2}{8\alpha}\frac{dp}{dx}\left(1-\frac{4}{3}\phi+\frac{1}{3}\phi^4\right) \tag{11}$$

Then, the velocity profile can be written in function of the average velocity as:

$$v = 2v_m\left(1-\frac{4}{3}\phi+\frac{1}{3}\phi^4\right)^{-1}\left(1-\frac{r^2}{R^2}\right) - 8v_m\frac{\tau_0}{R}\left(\frac{dp}{dx}\right)^{-1}\left(1-\frac{4}{3}\phi+\frac{1}{3}\phi^4\right)^{-1} \tag{12}$$

$$v = 2v_m\left(1-\frac{4}{3}\phi+\frac{1}{3}\phi^4\right)^{-1}\left\{\left(1-\frac{r^2}{R^2}\right) - 2\phi\left(1-\frac{r}{R}\right)\right\} \tag{13}$$

Equation (13) is valid for $R_p < r \leq R$.
The stress in the wall is:

$$\tau_w = \eta(\dot{\gamma})\ \dot{\gamma}|_{r=R} \tag{14}$$

The viscosity function for a Bingham ($\eta = \tau/\dot{\gamma}$) fluid is given by:

$$\eta(\dot{\gamma}) = \tau_0 \dot{\gamma}^{-1} + \alpha \tag{15}$$

Inserting (15) in (14):

$$\tau_w = (\tau_0 + \alpha\dot{\gamma})|_{r=R} = \left[\tau_0 + \alpha\left(\frac{dv}{dr}\right)\right]\Bigg|_{r=R} \tag{16}$$

Inserting Eq. (13) in (16):

$$\tau_w = \tau_0 - 4\alpha v_m \left(1 - \frac{4}{3}\phi + \frac{1}{3}\phi^4\right)^{-1}\left(\frac{1-\phi}{R}\right) \tag{17}$$

For the cylindrical case, the force in the wall can be obtained from the wall stress, relating the stress with the surface area of contact a_s. The extrapolated equation in the vector form is given by

$$\mathbf{f}_i = \left[2\pi L\tau_0 R_i |\mathbf{v}_{mi}|^{-1} - 8\alpha\pi L R_i v_{mi}\left(1 - \frac{4}{3}\phi_i + \frac{1}{3}\phi_i^4\right)^{-1}\left(\frac{1-\phi_i}{R_i}\right)\right]\mathbf{v_{mi}} \tag{18}$$

From Eq. (5), the interaction term is given by:

$$\mathbf{m}_f = \left[2\varepsilon\tau_0 \frac{\sum_{i=1}^N R_i}{\sum_{i=1}^N R_i^2}|\mathbf{v}_{mi}|^{-1} - 8\varepsilon\alpha\sum_{i=1}^N \frac{\left(1 - \frac{4}{3}\phi_i + \frac{1}{3}\phi_i^4\right)^{-1}(1-\phi_i)}{\sum_{i=1}^N R_i^2}\right]\mathbf{v_{mi}} \tag{19}$$

The interaction term can also be written in the function of mobility $\mathbf{M}$. So, the mobility tensor is given by:

$$\mathbf{M}^{-1} = \left[-\frac{2\tau_0}{\varepsilon}\frac{\sum_{i=1}^N R_i}{\sum_{i=1}^N R_i^2} + \frac{8\alpha}{\varepsilon}\sum_{i=1}^N \frac{\left(1 - \frac{4}{3}\phi_i + \frac{1}{3}\phi_i^4\right)^{-1}(1-\phi_i)}{\sum_{i=1}^N R_i^2}\mathbf{v_{mi}}\right]\mathbf{v_m}^{-1}\mathbf{I} \tag{20}$$

2.4 Calculating the velocity in the pores

The average velocity in a given pore is:

$$v_{f_i} = \frac{R_i^2}{8\alpha}\left(\frac{dp}{dx}\right)_i\left(1 - \frac{4}{3}\phi_i + \frac{1}{3}\phi_i^4\right) \tag{21}$$

The total flow rate in the REV is:

$$Q = v_m A_{total} = v_m \sum_{i=1}^N \pi R_i^2 \tag{22}$$

Also, the flow rate in the REV can be described as the sum of the flow rates in each pore:

$$Q = \sum_{i=1}^N q_i = \sum_{i=1}^N \pi v_i R_i^2 \tag{23}$$

Comparing (22) and (23), the average velocity in the REV can be written as:

$$v_m = \frac{\sum_{i=1}^N v_i R_i^2}{\sum_{i=1}^N R_i^2} \tag{24}$$

Inserting (21) in (24):

$$v_m = \frac{1}{8\alpha} \frac{\sum_{i=1}^{N} \left(\frac{dp}{dx}\right)_i \left(1 - \frac{4}{3}\phi_i + \frac{1}{3}\phi_i^4\right) R_i^4}{\sum_{i=1}^{N} R_i^2} \tag{25}$$

We use the hypothesis that the pressure gradient is the same in each pore. Then, the velocity in each pore is then given by:

$$v_{f_i} = R_i^2 \left(1 - \frac{4}{3}\phi_i + \frac{1}{3}\phi_i^4\right) \frac{\sum_{i=1}^{N} R_i^2}{\sum_{i=1}^{N} \left(1 - \frac{4}{3}\phi_i + \frac{1}{3}\phi_i^4\right) R_i^4} v_m \tag{26}$$

The interaction term can be written in the scalar form as:

$$m_f = 2\varepsilon\tau_0 \frac{\sum_{i=1}^{N} R_i}{\sum_{i=1}^{N} R_i^2} - 8\varepsilon\alpha \sum_{i=1}^{N} \frac{\left(1 - \frac{4}{3}\phi_i + \frac{1}{3}\phi_i^4\right)^{-1} (1 - \phi_i)}{\sum_{i=1}^{N} R_i^2} v_{mi} \tag{27}$$

Inserting (26) in (27):

$$m_f = 2\varepsilon\tau_0 \frac{\sum_{i=1}^{N} R_i}{\sum_{i=1}^{N} R_i^2} - 8\varepsilon\alpha \sum_{i=1}^{N} \frac{(1 - \phi_i) R_i^2}{\sum_{i=1}^{N} \left(1 - \frac{4}{3}\phi_i + \frac{1}{3}\phi_i^4\right) R_i^4} v_m \tag{28}$$

Extrapolating equation (28) to the vector form:

$$\mathbf{m}_f = \left[2\varepsilon\tau_0 \frac{\sum_{i=1}^{N} R_i}{\sum_{i=1}^{N} R_i^2} |\mathbf{v}_m|^{-1} - 8\varepsilon\alpha \sum_{i=1}^{N} \frac{(1 - \phi_i) R_i^2}{\sum_{i=1}^{N} \left(1 - \frac{4}{3}\phi_i + \frac{1}{3}\phi_i^4\right) R_i^4} \right] \mathbf{v}_m \tag{29}$$

Then, the inverse of the mobility tensor is:

$$\mathbf{M}^{-1} = \left[-\frac{2\tau_0}{\varepsilon} \frac{\sum_{i=1}^{N} R_i}{\sum_{i=1}^{N} R_i^2} + \frac{8\alpha}{\varepsilon} \sum_{i=1}^{N} \frac{(1 - \phi_i) R_i^2}{\sum_{i=1}^{N} \left(1 - \frac{4}{3}\phi_i + \frac{1}{3}\phi_i^4\right) R_i^4} \mathbf{v}_m \right] \mathbf{v}_m^{-1} \mathbf{I} \tag{30}$$

2.5 Numerical Formulation

The simulations were conducted utilizing OpenFOAM (Jasak, 2009), an open-source C++ library that employs the finite volume method.

The computational domain utilized in the simulations was a two-dimensional structured mesh comprised of hexahedral cells of uniform size. To optimize computational resources, a plug sector was considered in the flow direction. Moreover, at the domain entrance, a narrow region was initialized without a solid phase to ensure that the uniform flow boundary condition at the entrance does not significantly influence the preferred fluid path at the porous medium inlet.

For introducing heterogeneity representative of real plugs, the initial porosity field was randomly generated. The generated fields were replicated in other cases, ensuring that the initial fields did not impact the subsequent analysis. The porosity field generated for the simulated cases is illustrated in Fig. 1.

The applied boundary conditions are presented in Table [1].

Variable	Initial Condition	Inlet	Outlet	Walls
u	$u = 0$	$u = \hat{f}(Re)$	$\mathbf{n} \cdot \nabla u = 0$	*slip*
p	$p = 0$	$\mathbf{n} \cdot \nabla p = 0$	$p = 0$	$\mathbf{n} \cdot \nabla p = 0$

Table 1: Initial and boundary conditions applied to all cases.

The porosity-permeability relationship is obtained through a Carman-Kozeny relationship and the inverse of the permeability field is presented in Figure 2.

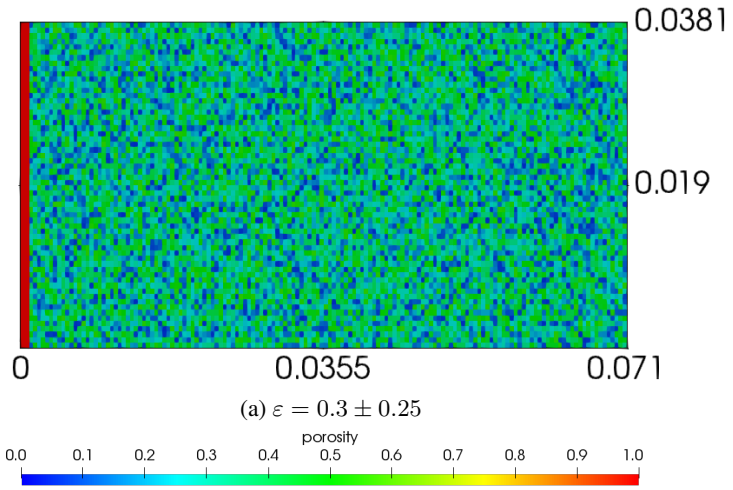

(a) $\varepsilon = 0.3 \pm 0.25$

Figure 1: Randomly generated porosity field for plug simulated cases.

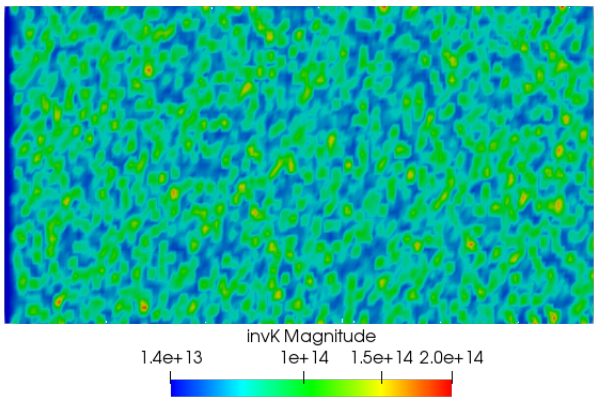

Figure 2: Inverse of permeability field for all cases.

3. RESULTS

The results are presented in function of Reynolds number, defined as

$$Re = \frac{\rho U L_c}{\eta_c}, \tag{31}$$

where L_c is the characteristic length given by $L_c = K/r_p$ (Motta *et al.*, 2021), η_c is the characteristic viscosity, ρ is the fluid density and U is the inlet velocity. The Bingham viscosity model evaluated at the characteristic shear rate is given by

$$\eta_c = \frac{\tau_0 r_p}{U} + \alpha. \tag{32}$$

The simulations also considered a constant plasticity number Pl (Thompson and Soares, 2016) given by:

$$Pl = \frac{\tau_0}{\tau_c} = \frac{\tau_0}{\tau_0 + \alpha\dot{\gamma}_c}, \tag{33}$$

where $\dot{\gamma}_c = \frac{U}{r_p}$ is the characteristic shear-rate. We have considered $Pl = 0.3$ for all simulations and Re values of 10^{-6}, 10^{-5} and 10^{-4}.

We have evaluated three Gaussian pore size distribution cases: $\sigma_0 = 0$ (no standard deviation, uniform distribution), $\sigma_1 = 0.2r_p$ and $\sigma_2 = 0.9r_p$, where the mean pore radius r_p is 10^{-6} is the same for all cases. Figure 3 shows the pressure

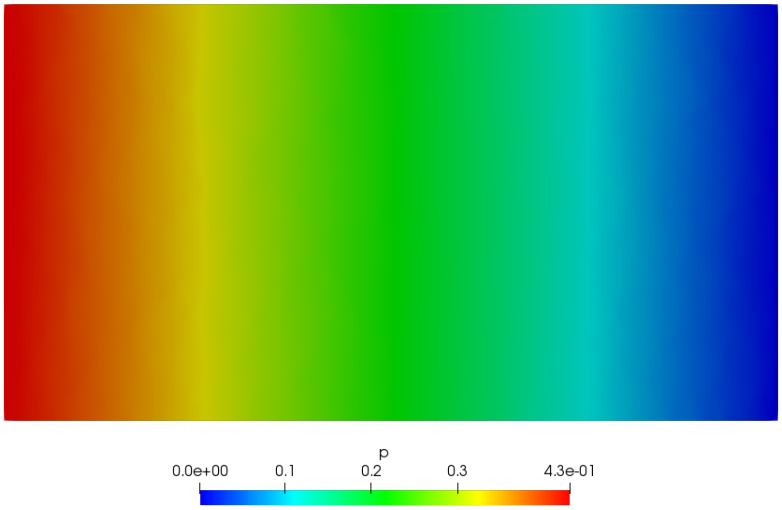

Figure 3: Pressure field for the case with $Re = 10^{-5}$ and $\sigma = 0.2r_p$.

field for the case with $Re = 10^{-5}$ and $\sigma_1 = 0.2r_p$. Pressure only varies in the flow direction. This is observed in all cases.

The pressure drop along the plug is compared for all cases in Figure 4. For cases with the same Re, the pressure drop is higher when no distribution is considered. As the heterogeneous intra-REV hypothesis is introduced, the pressure drop is lower for the σ_1 case and even lower for the σ_2 case. This behavior is expected because when a distribution of pores is considered, the presence of larger pores forms higher mobility regions, hence inducing a lower pressure drop. The effect is intensified when the standard deviation is increased. This trend is observed for all evaluated Re numbers and the pressure drop is reduced for lower Re numbers, as expected. These important results indicate that the classical single representative pore assumptions, present in many two-scale models in the literature may overestimate the pressure drop necessary to maintain the constant flow rate, even for a pore geometry that offers a high mobility, like the cylinder.

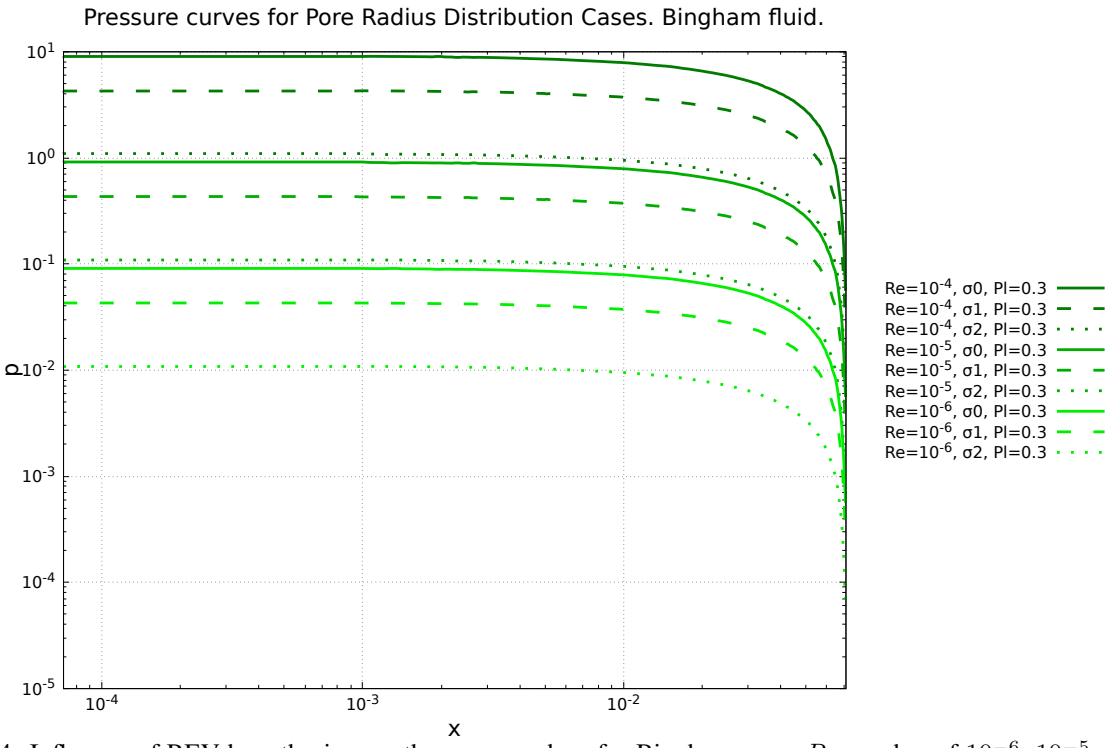

Figure 4: Influence of REV hypothesis over the pressure drop for Bingham case. Re number of 10^{-6}, 10^{-5} and 10^{-4}. $Pl = 0.3$.

The pressure drop was also evaluated in a dimensionless form,

$$p^* = \frac{p - p_e}{\frac{\eta_c U r_p}{K}}, \tag{34}$$

$$x^* = \frac{x}{L}, \tag{35}$$

where p^* is the dimensionless pressure drop, p_e is the pressure at the exit of the domain, x^* is the dimensionless coordinate in the flow direction and L is the plug length. Figure 5 shows the dimensionless pressure drop along the plug for the simulated cases. From the results, it can be seen that the dimensionless pressure drop does not depend on the Reynolds number, only on the distribution.

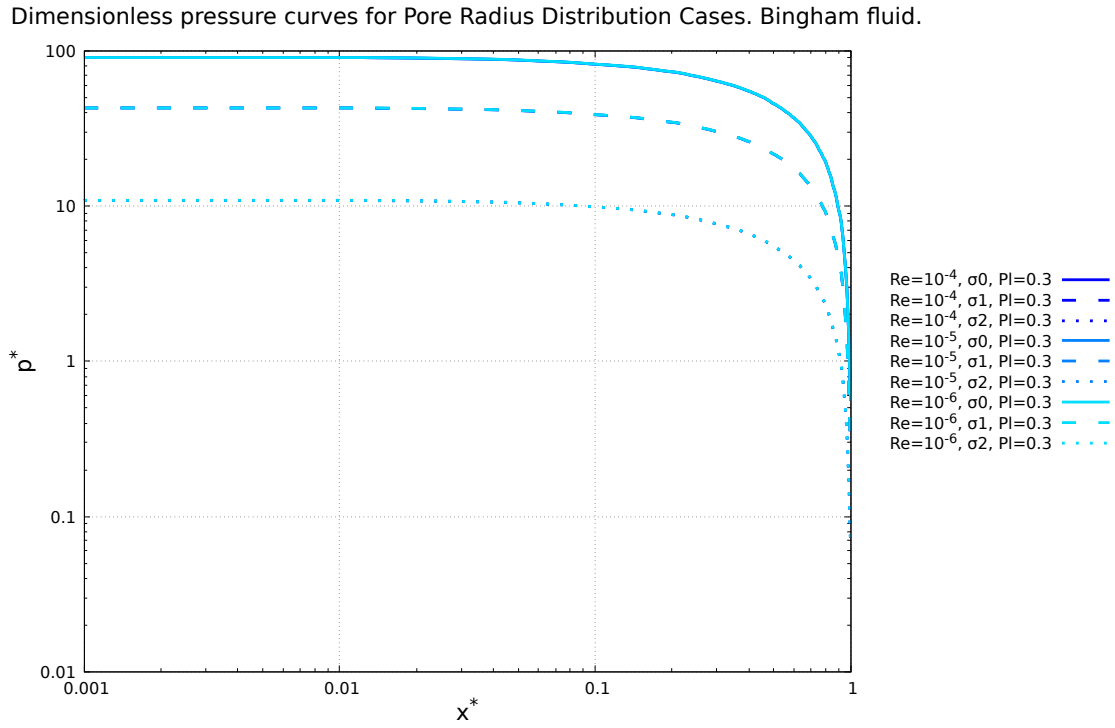

Figure 5: Influence of REV hypothesis over the dimensionless pressure drop for Bingham case. Re number of 10^{-6}, 10^{-5} and 10^{-4}. $Pl = 0.3$.

4. CONCLUSIONS

This work has an important contribution to the study of the flow of complex fluids through porous media, especially concerning two-scale models and Mixture Theory. We develop an analytical solid-fluid interaction term for a rigid porous medium and Bingham viscoplastic fluid model. The analytical development is also made to cases when the smallest scale is modeled not only by a single representative pore but also by a heterogeneous distribution of pores.

To evaluate the effectiveness of the approach, we conducted tests on viscoplastic non-Newtonian fluid flow within a porous medium plug, maintaining a constant flow rate. We considered Bingham material with a Pl number of 0.3. It is important to note that this form of heterogeneity differs from a heterogeneous porosity distribution. While we examined the impact of an intra-REV pore distribution, heterogeneous porosity pertains to an inter-REV characteristic. It is possible to achieve the same porosity value with either a uniform or non-uniform distribution of pores within a REV.

We observed that the pressure drop curves show a significant difference between homogeneous and heterogeneous pore distribution. When the intra-REV distribution is non-uniform, the pressure drop is lower and even lower when the standard deviation is increased, revealing a limitation of the single representative pore that may not be able to represent the pressure drop observed in plug experiments.

5. ACKNOWLEDGEMENTS

We would like to thank Conselho Nacional de Pesquisa e Desenvolvimento (CNPq) and Coordenação de Aperfeiçoamento de Pessoal de Nível Superior (CAPES) for financial support.

6. REFERENCES

Alleman, D., Qi, Q. and Keck, R., 2003. "The development and successful field use of viscoelastic surfactant-based diverting agents for acid stimulation". In *International symposium on oilfield chemistry*. OnePetro.

Atkin, R.J. and Craine, R.E., 1976. "Continuum theories of mixtures: Basic theory and historical development". *The Quartely Journal of Mechanics and Applied Mathematics*, Vol. 29, p. 209.

Cannella, W., Huh, C. and Seright, R., 1988. "Prediction of xanthan rheology in porous media". In *SPE annual technical conference and exhibition*. OnePetro.

Chang, F., Qu, Q., Frenier, W. *et al.*, 2001. "A novel self-diverting-acid developed for matrix stimulation of carbonate reservoirs". In *SPE international symposium on oilfield chemistry*. Society of Petroleum Engineers.

Fletcher, A., Flew, S., Lamb, S., Lund, T., Bjornestad, E., Stavland, A. and Gjovikli, N., 1991. "Measurements of polysaccharide polymer properties in porous media". In *SPE International Symposium on Oilfield Chemistry*. OnePetro.

Golfier, F., Zarcone, C., Bazin, B., Lenormand, R., Lasseux, D. and QUINTARD, M., 2002. "On the ability of a darcy-scale model to capture wormhole formation during the dissolution of a porous medium". *Journal of fluid Mechanics*, Vol. 457, pp. 213–254.

Jasak, H., 2009. "Openfoam: open source cfd in research and industry". *International Journal of Naval Architecture and Ocean Engineering*, Vol. 1, No. 2, pp. 89–94.

Liu, X., Ormond, A., Bartko, K., Ying, L. and Ortoleva, P., 1997. "A geochemical reaction-transport simulator for matrix acidizing analysis and design". *Journal of Petroleum Science and Engineering*, Vol. 17, No. 1-2, pp. 181–196.

Lopez, X., Valvatne, P.H. and Blunt, M.J., 2003. "Predictive network modeling of single-phase non-newtonian flow in porous media". *Journal of colloid and interface science*, Vol. 264, No. 1, pp. 256–265.

Maheshwari, P., Ratnakar, R.R., Kalia, N. and Balakotaiah, V., 2013. "3-d simulation and analysis of reactive dissolution and wormhole formation in carbonate rocks". *Chemical Engineering Science*, Vol. 90, p. 258.

Motta, A.B., Thompson, R.L., Favero, J.L., Dias, R.A., Silva, L.F., Costa, F.G. and Schwalbert, M.P., 2021. "Rheological effects on the acidizing process in carbonate reservoirs". *Journal of Petroleum Science and Engineering*, p. 109122.

Motta, A.B., Thompson, R.L., Schwalbert, M.P., Silva, L.F., Favero, J.L., Dias, R.A. and Leitão, R.J., 2022. "Effects of intra-rev pore distribution modeling in the flow of non-newtonian fluids in porous media". *Transport in Porous Media*, Vol. 145, No. 2, pp. 505–525.

Nasr-El-Din, H.A., Chesson, J.B., Cawiezel, K.E. and De Vine, C.S., 2006. "Lessons learned and guidelines for matrix acidizing with viscoelastic surfactant diversion in carbonate formations". In *SPE Annual Technical Conference and Exhibition*. OnePetro.

Panga, M.K.R., Ziauddin, M. and Balakotaiah, V., 2005. "Two-scale continuum model for simulation of wormholes in carbonate acidization". *AIChE Journal*, Vol. 51, pp. 3231–3248. doi:10.1002/aic.10574.

Ratnakar, R.R., Kalia, N. and Balakotaiah, V., 2013. "Modeling, analysis and simulation of wormhole formation in carbonate rocks with in situ cross-linked acids". *Chemical Engineering Science*, Vol. 90, pp. 179–199.

Siddiqui, S., Nasr-El-Din, H.A. and Khamees, A.A., 2006. "Wormhole initiation and propagation of emulsified acid in carbonate cores using computerized tomography". *Journal of Petroleum Science and Engineering*, Vol. 54, No. 3-4, pp. 93–111.

Thompson, R.L. and Soares, E.J., 2016. "Viscoplastic dimensionless numbers". *Journal of Non-Newtonian Fluid Mechanics*, Vol. 238, pp. 57–64.

Wang, Y., Hill, A. and Schechter, R., 1993. "The optimum injection rate for matrix acidizing of carbonate formations". In *SPE Annual Technical Conference and Exhibition*. OnePetro.

Willhite, G.P. and Uhl, J., 1988. "Correlation of the flow of flocon 4800 biopolymer with polymer concentration and rock properties in berea sandstone". In *Water-Soluble Polymers for Petroleum Recovery*, Springer, pp. 101–119.

7. RESPONSIBILITY NOTICE

The authors are solely responsible for the printed material included in this paper.